arXiv:0705.0947v1 [hep-ph] 7 May 2007

STRING JUNCTION AND DIFFUSION OF BARYON CHARGE IN MULTIPARTICLE PRODUCTION PROCESSES

Yu. M. Shabelski

Petersburg Nuclear Physics Institute, Gatchina, St. Petersburg, Russia

Lecture given at XXXX PNPI Winter School of Physics, Repino, St.Petersburg, February 2006

A b s t r a c t

We consider the phenomenological consequences of the assumption that the baryons are the systems of three quarks and string junction. The process of baryon number transfer due to string junction propagation in rapidity space is considered in detail. At high energies it leads to a significant effect in the net baryon production in hN and hA collisions at mid-rapidities and in the incident meson fragmentation region. The results of numerical calculations in the framework of the Quark–Gluon String Model are in reasonable agreement with the data.

PACS. 25.75.Dw Particle and resonance production

E-mail: shabelsk@thd.pnpi.spb.ru

1 Introduction

The Quark–Gluon String Model (QGSM) and the Dual Parton Model (DPM) are based on the Dual Topological Unitarization (DTU) and describe quite reasonably many features of high energy production processes, in both hadron–nucleon and hadron–nucleus collisions [1]–[7]. High energy interactions are considered as going via the exchange of one or several Pomerons, and all elastic and inelastic processes result from cutting through or between Pomerons [8]. Inclusive spectra of hadrons are related to the corresponding fragmentation functions of quarks and diquarks, which are constructed using the Reggeon counting rules [9].

In the present lecture, we discuss the processes connected with the transfer of baryon charge over long rapidity distances. In the string models, baryons are considered as configurations consisting of three strings (related to three valence quarks) connected at the point called "string junction" (SJ) [10]–[14]. The string junction has a nonperturbative origin in QCD. Many phenomenological results were obtained 25 years ago [11, 12], [15]–[19]. They are discussed shortly in Sect. 2.

It is very important to understand the role of the string junction in the dynamics of high-energy hadronic interactions. Now we have several different experimental results concerning the processes of baryon charge transfer.

The most impressive are the data [20] on $\Omega/\bar{\Omega}$ asymmetry in collisions of particles without strange quarks in the initial state. This asymmetry is absent in many phenomenological models. It appears as a result of SJ existing in the initial state and it was predicted qualitatively in [19].

The data [21] clearly show that in the forward hemisphere the number of secondary protons produced in $\pi^+ p$ interactions is significantly larger than the number of secondary antiprotons produced in $\pi^- p$ collisions. This difference cannot be described [6] without the assumption that the baryon charge is transferred from the target proton to the pion hemisphere.

There exist the data obtained on nuclear targets. The discussed effects are confirmed by the measurements of $\Lambda/\bar{\Lambda}$ and $\Xi/\bar{\Xi}$ hyperon production asymmetries in 500 GeV/c π^--nucleus interactions [20]. Similar data on the differences of $p - \bar{p}$ yields in $\frac{1}{2}(\pi^+ p + \pi^- p)$ collisions together with the same data for Pb target at 158 GeV/c were presented by the NA49 Coll. [22]. The data [23] on hyperon production by π^- beam on carbon and copper targets show the evident and numerically large difference in the spectra of secondary baryons

and antibaryons.

A second group of data concerns the energy dependence of the differences in yields of the protons and antiprotons at 90° (*i.e.* at $x_F = 0$) at ISR energies [24]. Similar data on $\bar{p}/p$ ratio at RHIC energies [25, 26] were published recently. Finally, the proton–antiproton asymmetry in photoproduction was measured at HERA [27].

Quantitative theoretical description of baryon number transfer via string junction mechanism was suggested in 90's. In [28], the experimentally observed $p/\bar{p}$ asymmetry at HERA energies was predicted that was confirmed by the data [27] which were obtained later. This asymmetry was considered in more detail in [29, 30]. In [31], it was noted that the $p/\bar{p}$ asymmetry measured at HERA can be obtained by simple extrapolation of ISR data.

The important theoretical results on the baryon number transfer due to SJ diffusion in rapidity space were obtained in [32] and following papers [33]–[36]. In the present lecture, we consider the main results for the case of secondary baryon/antibaryon production both from nucleon and nuclear targets.

The most interesting are the differences in baryon and antibaryon production in the meson beam fragmentation. In the case of nuclear target the discussed effects are enhanced due to two reasons. First, the usual production of secondaries (which can be considered as a background for string junction effects) in the beam fragmentation region is suppressed due to nuclear absorption [5],[37–39]. Second, the probability of the baryon number transfer should be proportional to the number of inelastic interactions in the nuclear matter, $\langle\nu\rangle_{hA}$.

In the case of baryon beams the SJ effects are the most important in the central (midrapidity) region [32, 33].

2 Baryon as $3q + SJ$ system

In QCD, the hadrons are composite bound state configurations built up from the quark $\psi_i(x), i = 1, ...N_c$ and gluon $G^\mu_a(x)$, $a = 1, ..., N_c^2 - 1$ fields. In the string models the meson wave function has the form of "open string" [10, 12], as is shown in Fig. 1a.

The meson wave function reads as follows:

$$M \;=\; \bar{\psi}^i(x_1)\Phi^{i'}_i(x_1, x_2)\psi_{i'}(x_2)\,, \qquad (1)$$

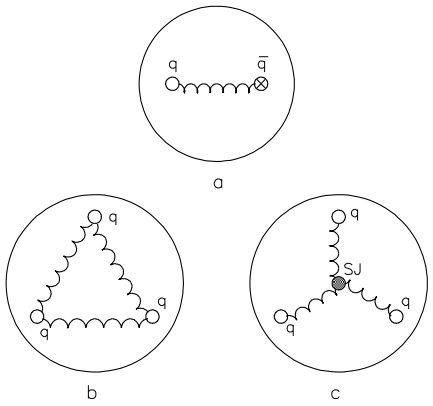


Figure 1: Composite structure of a meson (a) and baryon (b) and (c) in string models. Quarks are shown by open points and antiquarks by crossed points

$$\Phi_i^{i'}(x_1, x_2) = \left[T \exp \left(g \int\limits_{P(x_1,x_2)} A_\mu(z) dz^\mu \right) \right]_i^{i'} . \tag{2}$$

In the last equation $P(x_1, x_2)$ represents a path from x_1 to x_2 which looks like an open string with ends in x_1 and x_2.

For the baryons there exist two possibilities, "triangle", or Δ connection shown in Fig. 1b and "star", or Y connection shown in Fig. 1c. The last variant is considered as the most interesting. Here a baryon is considered as configurations consisting of three strings attached to three valence quarks and connected in a point called the "string junction" (SJ) [10, 12]. The correspondent wave function can be written as

$$B = \psi_i(x_1)\psi_j(x_2)\psi_k(x_3)J^{ijk} , \tag{3}$$

$$J^{ijk} = \Phi^i_{i'}(x_1, x)\Phi^j_{j'}(x_2, x)\Phi^k_{k'}(x_3, x)\epsilon^{i'j'k'} . \tag{4}$$

Such baryon wave function can be defined as a "star" or "Y" shape and it is preferable [10, 12] in comparison with "triangle" ("ring") or "Δ" shape, where the problems with gauge invariance appear [12]. This "Y" structure of baryon is confirmed by lattice calculations [40].

The presented picture leads to several phenomenological predictions.

In particular, there exist the rooms for exotic states, such as glueball, or

gluonium ("closed string"), Fig. 2a, [12, 41]

$$\text{Glueball} = \text{Tr}\left[T\exp\left(g\int\limits_{P(closed)} A_\mu(z)dz^\mu\right)\right]. \qquad (5)$$

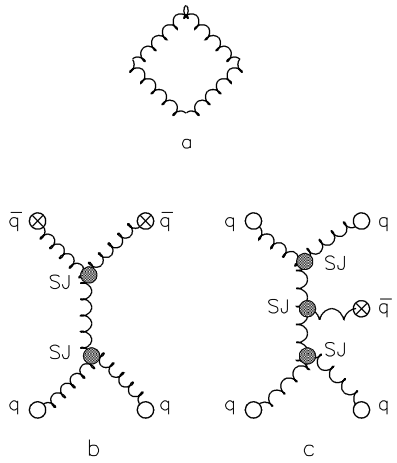


Figure 2: Exotic states: glueball (a), 4-quark meson (tetraquark) $M_4 = qq\bar{q}\bar{q}$ (b) and 5-quark baryon (pentaquark) $B_5 = qqqq\bar{q}$ (c) in string models. Quarks are shown by open points and antiquarks by crossed points

The multiquark bound states, such as 4-quark meson, Fig. 2b, pentaquark, Fig. 2c, *etc.* also can exist [12], [42]–[44]. Without specifying the model it is impossible to say anything definite about the sign of the correspondent binding energy, *i.e.* are they the bound states or not. However we can expect that the part of a particle momentum carried out by gluons in the case of multiquark states should be larger than for usual particles, Figs. 1a and 1c, due to the larger number of string junctions.

From the point of view of the Additive Quark Model, a meson consists, as before, of two constituent quarks, Fig. 1a, but a baryon consists now of four constituent objects, three constituent quarks and SJ, as is shown in Fig. 1c. In such a picture the ratio of nucleon–nucleon and meson–nucleon total cross sections at high energies increases [18] as compared to classical result [45] $\sigma(N-N)/\sigma(\pi-N) = 3/2$, namely, with accounting for the possibility of SJ interaction with a target

$$\frac{\sigma(N-N)}{\sigma(\pi-N)} \;=\; \frac{3}{2} + \frac{\sigma(SJ-N)}{2\sigma(q-N)}\,, \qquad (6)$$

where the additional term $\sigma(SJ{-}N)/(2\sigma(q{-}N))$ can be estimated [18] to equal $1/4 \div 1/6$. This correction results in a better agreement [46] with experimental data.

The $B\bar{B}$ annihilation cross section, σ_{ann}, is not necessarily equal to the difference $\Delta\sigma = \sigma^{tot}(B\bar{B}) - \sigma^{tot}(BB)$ [12].

The existence of SJ in a baryon structure changes the quark counting rules for reactions with large momenta transfer [15, 19]. The reaction $\bar{p}p \to \bar{\Omega}\Omega$ can occur now without breaking the OZI rules. The ratio of $\bar{\Omega}/\Omega$ production for the collisions of non-strange hadrons is predicted to be smaller than unity [19] contrary to many models for multiparticle production. This prediction is in agreement with the experimental data [20] and their model description in [32, 33].

In the case of inclusive reactions the baryon number transfer to large rapidity distances in hadron–nucleon reactions can be explained by SJ diffusion [28, 32]. Now we consider several examples of effects connected with the string junction diffusion for hadron–nucleon and hadron–nucleus inelastic interactions.

3 Inclusive spectra of secondary hadrons in the Quark–Gluon String Model

For more quantitative predictions we need certain model for multiparticle production and we will use the QGSM for the numerical predictions presented below.

As was mentioned above, the high energy hadron–nucleon and hadron–nucleus interactions are considered in the QGSM as going via the exchange of one or several Pomerons. Each Pomeron corresponds to a cylindrical diagram, see Fig. 3a, thus, when cutting a Pomeron, two showers of secondaries are produced as is shown in Fig. 3b. The inclusive spectrum of secondaries is determined by the convolution of diquark, valence quark and sea quark distributions $u(x, n)$ in the incident particles and the fragmentation functions $G(z)$ of quarks and diquarks into secondary hadrons. The diquark and quark distribution functions depend on the number n of cut Pomerons in the considered diagram.

For nucleon target, the inclusive spectrum of a secondary hadron h has the

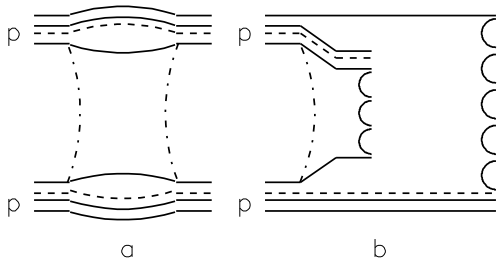


Figure 3: Cylindrical diagram corresponding to the one–Pomeron exchange contribution to elastic pp scattering (a) and its cut which determines the contribution to inelastic pp cross section (b). Quarks are shown by solid curves and SJ by dashed curves

form [1]:

$$\frac{x}{\sigma_{inel}}\frac{d\sigma}{dx} \;=\; \sum_{n=1}^{\infty} w_n \phi_n^h(x) \;, \tag{7}$$

where the functions $\phi_n^h(x)$ determine the contribution of diagrams with n cut Pomerons and w_n is the probability of this process. Here we neglect the contributions of diffraction dissociation processes which are comparatively small in the majority of processes considered below. They can be separately accounted for [1, 3, 6].

For pp collisions

$$\begin{aligned} \phi_{pp}^h(x) &= f_{qq}^h(x_+,n) f_q^h(x_-,n) + f_q^h(x_+,n) f_{qq}^h(x_-,n) \\ &\qquad + 2(n-1) f_s^h(x_+,n) f_s^h(x_-,n) \;, \qquad (8) \\ x_\pm &= \frac{1}{2}\left[\sqrt{4m_T^2/s + x^2} \;\pm x\right], \qquad (9) \end{aligned}$$

where f_{qq}, f_q and f_s correspond to the contributions of diquarks, valence and sea quarks respectively.

The last functions are determined by the convolution of the diquark and quark distributions with the fragmentation functions, for example,

$$f_q^h(x_+,n) \;=\; \int_{x_+}^{1} u_q(x_1,n) G_q^h(x_+/x_1) dx_1 \;. \tag{10}$$

For meson beam the diquark contribution $f_{qq}^h(x_+,n)$ in Eq. (8) should be

changed by the contribution of valence antiquarks:

$$\phi^h_{\pi p}(x) = f^h_{\bar{q}}(x_+,n) f^h_q(x_-,n) + f^h_q(x_+,n) f^h_{qq}(x_-,n) + 2(n-1) f^h_s(x_+,n) f^h_s(x_-,n)\,. \tag{11}$$

The diquark and quark distributions as well as the fragmentation functions are determined by Regge intercepts.

According to [32, 33], we consider three possibilities to obtain the net baryon charge. The first one is the fragmentation of the diquark giving rise to a leading baryon (Fig. 4a). A second possibility is to produce a (leading) meson in the first break-up of the string and baryon in the subsequent break-up (Fig. 4b). In the considered approach the baryon consists of three valence quarks together with string junction (SJ), which is conserved during the interaction.[1] This gives a third possibility for secondary baryon production in non-diffractive hadron–nucleon interactions, shown in Fig. 4c.

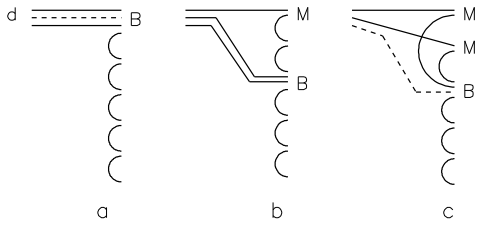


Figure 4: QGSM diagrams describing secondary baryon B production by diquark d: initial SJ together with two valence quarks and one sea quark (a), together with one valence quark and two sea quarks (b) and together with three sea quarks (c)

In Fig. 4a, the secondary baryon consists of the SJ together with two valence (qq) and one sea (s) quarks, in Fig. 4b of one valence and two sea quarks and in Fig. 4c of three sea quarks. The corresponding fragmentation functions for the secondary baryon B production can be written as follows (see [32, 33] for more detail):

$$G^B_{qq}(z) = a_N v_{qq} z^{2.5}\,, \tag{12}$$

$$G^B_{qs}(z) = a_N v_{qs} z^2 (1-z)\,, \tag{13}$$

$$G^B_{ss}(z) = a_N \varepsilon v_{ss} z^{\alpha_{SJ}-1} (1-z)^2 \tag{14}$$

for the processes shown in Figs. 4a, 4b and 4c, respectively. The fraction z of the incident baryon energy carried by the secondary baryon increases

[1] At very high energies one or even several SJ pairs can be produced.

from Fig. 4a to Fig. 4c, whereas the mean rapidity gap between the incident and secondary baryon increases. In Eqs. (12)–(14), a_N is the normalization parameter for secondary baryon production, v_{qq}, v_{qs} and v_{ss} are the relative probabilities for different baryon production, they can be found from quark combinatorics [48, 49]. The contribution of the graph in Fig. 4c has a small coefficient ε and α_{SJ} is a parameter of Regge-trajectory for SJ exchange.

The probability to find a comparatively slow SJ in the case of Fig. 4c can be estimated from the data on the $\bar{p}p$ annihilation into mesons [18, 50]. This probability is known experimentally at comparatively small energies only where it is proportional to $s^{\alpha_{SJ}-1}$ with $\alpha_{SJ} \sim 0.5$. However, it has been argued [50] that the annihilation cross section contains a small piece which is independent of s and thus $\alpha_{SJ} \sim 1$.

In [32] the value $\alpha_{SJ} = 0.5$ was used. However, for such value of α_{SJ} different values of ε were needed for the description of the experimental data at moderate and high energies. This problem was solved in [33], where it was shown with the help of the new experimental data that all the data can be described with the parameter values

$$\alpha_{SJ} \,=\, 0.9\,, \quad \varepsilon \,=\, 0.024\,. \tag{15}$$

In the situation when two valence quarks of the incident diquark fragment into different secondaries (Figs. 4b and 4c) there exist mesons M which consist from an initial valence quark and sea antiquark. In the case shown in Fig. 4b these exists one such meson and in the case of Fig. 4c two such mesons are produced. The fragmentation function of a meson M in Fig. 4b was accounted for in all previous calculations in the framework of the QGSM [1]–[7] (see also [51]). The same fragmentation function can be used to account for the production of one meson M in Fig. 4c. To account for the production of the second meson M in Fig. 4c we need the additional fragmentation function which can be written as

$$G^M(z) \;=\; 8\varepsilon a_0 z^2(1-z)^2\;. \tag{16}$$

The value of the factor $8\varepsilon a_0$ is determined by normalization condition.

It is necessary to note that the process shown in Fig. 4c can be realized very naturally in the quark combinatoric approach [48] with the specified probabilities of a valence quark recombination (fusion) with sea quarks and antiquarks.

4 Comparison with the data on nucleon target

The processes of the baryon charge transfer (Fig. 4c) were not accounted for in papers [1],[3–6]. So first of all we present the description of data for secondary baryon production which were described earlier without SJ contribution. The results for secondary meson and antibaryon production are the same as before, the accounting for additional mesons M production in the process Fig. 4c gives numerically small correction.

The inclusive spectra of secondary protons produced in pp collisions at lab. energies 100 and 175 GeV [21] are shown in Fig. 5a together with the curves calculated in the QGSM. The difference of the calculated results with and without SJ contribution is small here.

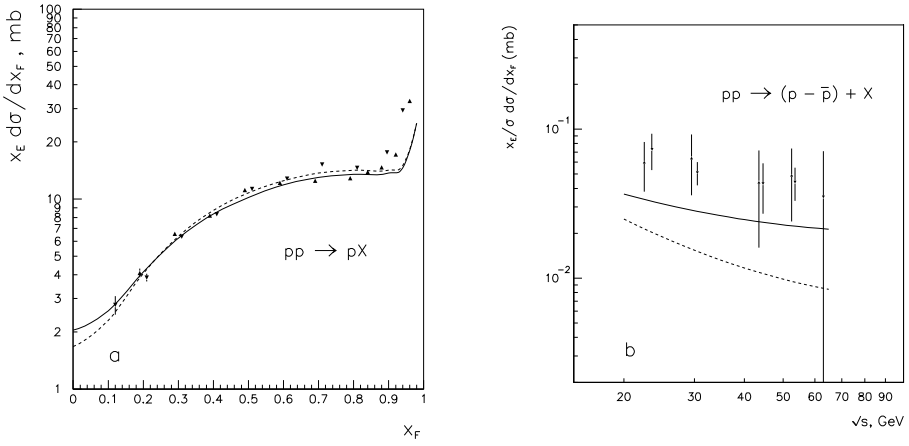


Figure 5: Spectra of secondary protons produced in pp collisions at 100 and 175 GeV/c [21] (a). The difference of the spectra of secondary protons and antiprotons produced in pp collisions at ISR energies [24] at 90^o in c.m.s. (b). The QGSM description with $\varepsilon = 0.024$ and with $\varepsilon = 0$ are shown by solid and dashed curves, respectively

The data on secondary proton and antiproton production in pp collisions at ISR energies [24] at 90^o in c.m.s. were obtained in [24]. Their differences, which are more sensitive to the baryon charge transfer, are presented in Fig. 5b. Now the effects of SJ contribution are more important. One can see that the last data are described quite reasonably by QGSM with $\varepsilon = 0.024$, whereas the calculations without SJ contributions underestimate the data. However, it is necessary to note that the systematical errors in [24] are of the order of 30%, and there exists the disagreement between the data [21], [52] and [24] of the order of 20–30%.

There exist only a few data on secondary production in pp collisions at RHIC energies. In Fig. 6, we present the rapidity (in c.m.) distribution of the ratio $\bar{p}/p$ in pp interactions at $\sqrt{s} = 200\,\mathrm{GeV}$ [25]. The QGSM calculation with the SJ contribution (15) (solid curve) is in reasonable agreement with the data, and the same calculation without SJ contributions (dashed curve) overestimates the discussed ratios.

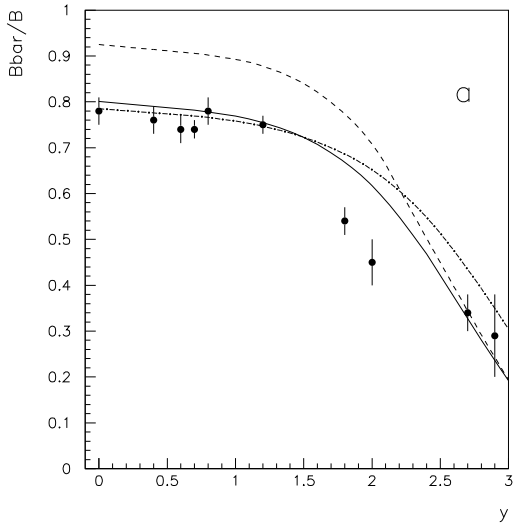


Figure 6: Rapidity dependence of $\bar{p}/p$ ratios for pp collisions at $\sqrt{s} = 200\,\mathrm{GeV}$. Solid and dashed curves show the QGSM description with and without SJ contribution and dash-dotted curve shows the QGSM predictions for $\bar{\Lambda}/\Lambda$ ratio

It is important to note that at asymptotic energies the ratio $\bar{p}/p$ is equal to the unity. So the deviation of the discussed ratio from the unity can appear due to some physical reason. One can see from Fig. 6 that the SJ contribution changes the deviation of $\bar{p}p$ from unity at small y, *i.e.* in the central region about three times in comparison with the calculation without SJ contribution.

The dash-dotted curve in Fig. 6 shows the QGSM with SJ contribution predictions for $\bar{\Lambda}/\Lambda$ ratios at RHIC energies. The spectra of secondary Λ produced in pp collisions at fixed target energies depend rather weakly on the SJ diffusion effects, as one can see in [32]. The QGSM calculations [33] predict practically equal values of $\bar{B}/B$ ratios in midrapidity region for all strange baryons that is qualitatively confirmed by the RHIC data on $Au - Au$ collisions [47].

The data of baryon production in the pion fragmentation region are more sensitive to the SJ contribution in comparison with pp collisions. Significant

effects come from the possibility of the baryon number to transfer from the target nucleon to the beam fragmentation region. The existing data for secondary antinucleon production [21] are presented in Fig. 7. The spectra of antiprotons produced in $\pi^- p$ collisions shown in Fig. 7a allow one to fix the fragmentation function of quark into baryon/antibaryon. Were the contribution of the baryon charge transfer negligibly small, the inclusive spectra of reactions $\pi^- p \to \bar{p} X$ and $\pi^+ p \to pX$ in the pion fragmentation region would be practically the same [6]. Actually, the data for the second reaction are significantly higher than for the first one providing evidence for the baryon charge transfer due to the SJ diffusion. The difference of the inclusive spectra in the two considered processes allows one to estimate quantitatively the contribution of the baryon charge transfer. The QGSM calculations with accounting for SJ contribution are in better agreement with the data. The experimental data for secondary Λ and $\bar{\Lambda}$ production in πp and Kp collisions also are in agreement [34, 35] with the discussed approach predictions, but the experimental error bars are rather large.

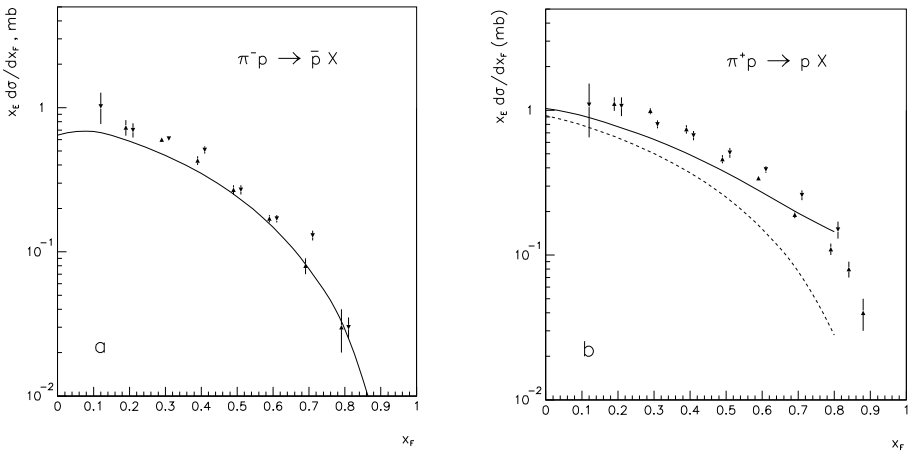


Figure 7: The spectra of secondary antiprotons in $\pi^- p$ collisions (a) and of protons in $\pi^+ p$ collisions (b) at lab. energies 100 and 175 GeV [21]. The QGSM description with $\varepsilon = 0.024$ and with $\varepsilon = 0$ in (b) is shown by solid curve and by dashed curve, respectively

In Fig. 8, we show the data [20] on the asymmetry of strange baryons

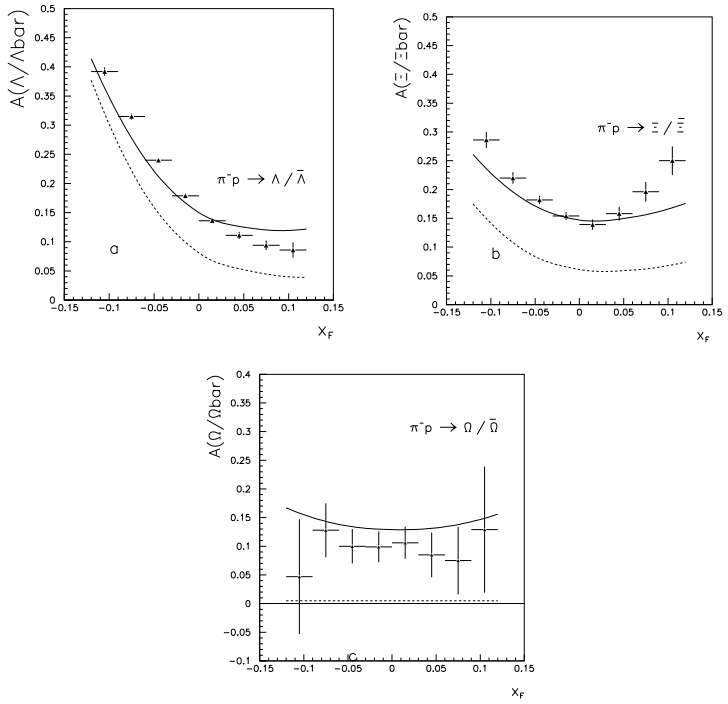


Figure 8: The asymmetries of secondary $\Lambda/\bar{\Lambda}$ (a), $\Xi^-/\overline{\Xi}^+$ (b), and $\Omega/\bar{\Omega}$ (c), in $\pi^- p$ collisions at 500 GeV/c [20] and its description by QGSM model. For all cases the calculations with $\epsilon = 0.024$ are shown by solid curves and the variants with $\epsilon = 0$ are shown by dashed curves

produced in π^- interactions [2] at 500 GeV/c. The asymmetry is determined as

$$A(B/\bar{B}) \;=\; \frac{N_B - N_{\bar{B}}}{N_B + N_{\bar{B}}} \tag{17}$$

for each x_F bin.

Theoretical curves for the data on all asymmetries calculated with $\varepsilon = 0.024$ are in reasonable agreement with the data. In case of $\Omega/\bar{\Omega}$ production we predict, following [19], a non-zero asymmetry in agreement with experimental data. Let us note that the last asymmetry is absent, say, in the naive quark model or in recombination model because Ω and $\bar{\Omega}$ have no common valence quarks with the incident particles.

[2] These data were obtained from pion interactions on a nuclear target where different materials were used in a very complicated geometry. We assume that the nuclear effects are small in the asymmetry and compare the pion-nucleus data with calculations for $\pi^- p$ collisions.

Preliminary data on $p/\bar{p}$ asymmetry in ep collisions at HERA were presented by the H1 Collaboration [27]. Here the asymmetry is defined as

$$A_B \;=\; 2\frac{N_p - N_{\bar{p}}}{N_p + N_{\bar{p}}}\,, \tag{18}$$

i.e. with an additional factor 2 in comparison with Eq. (17). The experimental value of A_B is equal to $(8.0 \pm 1.0 \pm 2.5)\%$ [27] for secondary baryons produced at $x_F \sim 0.04$ in the γp c.m. frame. QGSM without SJ contribution, *i.e.* with $\varepsilon = 0$ predicts here only 2.9 %, which is significantly smaller than the experimental value, whereas the calculation with $\varepsilon = 0.024$ gives the value 9.9 %, in good agreement with data.

5 Production of secondaries from nuclear targets in QGSM

As was mentioned above, the high energy hadron–nucleon and hadron–nucleus interactions are considered in the QGSM and in DPM as proceeding via the exchange of one or several Pomerons. Each Pomeron corresponds to a cylindrical diagram, and thus, when cutting a Pomeron, two showers of secondaries are produced. The inclusive spectrum of secondaries is determined by the convolution of diquark, valence quark and sea quark distributions $u(x, n)$ in the incident particles and the fragmentation functions $G(z)$ of quarks and diquarks into secondary hadrons.

The diquark and quark distribution functions depend on the number n of cut Pomerons in the considered diagram. In what follows we use the formalism of QGSM described in Section 3.

In the case of nuclear targets we should consider the possibility of one or several Pomeron cuts in each of the ν blobs of hadron–nucleon inelastic interactions as well as cuts between Pomerons. For example, for the πA collision one of the cut Pomerons links with valence antiquark and the valence quark of the projectile pion with valence quark and diquark of one target nucleons. The other Pomerons link with the sea quark–antiquark pairs of the projective pion with diquarks and valence quarks of another target nucleons and with sea quark–antiquark pairs of the target.

For example, one of the diagram for inelastic interaction with two target nucleons is shown in Fig. 9. In the blob of the πN_1 inelastic interaction one

Pomeron is cut, and in the blob of πN_2 interaction two Pomerons are cut. It is essential to take into account every possible Pomeron configuration and permutation for all diagrams. The process shown in Fig. 9 satisfies the condition [37] that the absorptive parts of hadron–nucleus amplitude are determined by the combinations of the absorptive parts of hadron–nucleon interactions.

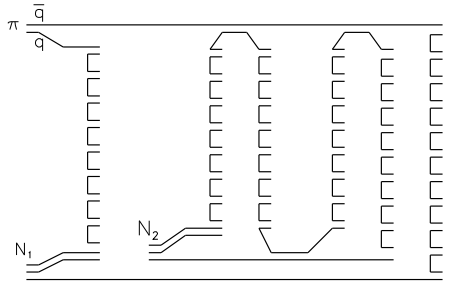


Figure 9: One of the diagrams for inelastic interaction of incident pion with two target nucleons N_1 and N_2 in πA collision

In the case of inelastic interactions with ν target nucleons, let n be the total number of cut Pomerons in hA collisions ($n \geq \nu$) and let n_i be the number of cut Pomerons connecting with the i-th target nucleon ($1 \leq n_i \leq n-\nu+1$). We define the relative weight of the contribution with n_i cut Pomerons in every hN blob as $w_{n_i}^{hN}$. For the inclusive spectrum of the secondary hadron h produced in a πA collision we obtain [5]

$$\begin{aligned}\frac{x_E}{\sigma_{\pi A}^{prod}}\frac{d\sigma}{dx_F} &= \sum_{\nu=1}^{A} V_{\pi A}^{(\nu)} \left\{ \sum_{n=\nu}^{\infty} \sum_{n_1=1}^{n-\nu+1} \cdots \sum_{n_\nu=1}^{n-\nu+1} \prod_{l=1}^{\nu} w_{n_l}^{\pi N} \right. \\ &\times \left[f_{\bar{q}}^h(x_+,n) f_q^h(x_-,n_l) + f_q^h(x_+,n) f_{qq}^h(x_-,n_l) \right. \\ &+ \left. \left. \sum_{m=1}^{2n-2} f_s^h(x_+,n) f_{qq,q,s}^h(x_-,n_m) \right] \right\}, \end{aligned} \tag{19}$$

where $V_{pA}^{(\nu)}$ is the probability of "pure inelastic" (nondiffractive) interactions with ν target nucleons, and we should account for all possible Pomeron permutation and the difference in quark content of the protons and neutrons in the target.

In particular, the contribution of the diagram in Fig. 9 to the inclusive spectrum is

$$\frac{x_E}{\sigma_{\pi A}^{prod}}\frac{d\sigma}{dx_F} = 2V_{\pi A}^{(2)} w_1^{\pi N_1} w_2^{\pi N_2}\Big\{ f_{qq}^h(x_+,3) f_q^h(x_-,1) + f_q^h(x_+,3) f_{qq}^h(x_-,1) + f_s^h(x_+,3)\Big[f_{qq}^h(x_-,2) + f_q^h(x_-,2) + 2f_s^h(x_-,2)\Big]\Big\}. \quad (20)$$

In the case of a nucleon beam the valence antiquark contributions of incident particle should be substituted by the contribution of valence diquarks.

The diquark and quark distributions as well as the fragmentation functions are here the same as in the case of the nucleon target (see Section 3). We account all three possibilities that the secondary baryon can consist of the SJ together with two valence and one sea quarks (Fig. 4a), with one valence and two sea quarks (Fig. 4b) or with three sea quarks (Fig. 4c).

In the present calculations, following the present experimental data, we increase the portion of strange quarks in the sea, S/L [32, 49] from $S/L = 0.2$ to $S/L = 0.32$.

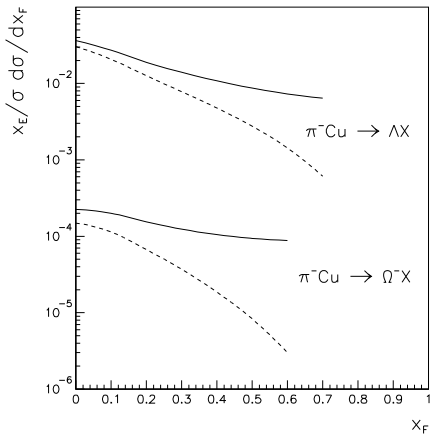


Figure 10: The QGSM predictions for the inclusive cross sections of Λ and Ω^- production in π^-Cu collisions at 400 GeV/c with (solid curves) and without (dashed curves) SJ contributions

To illustrate the expected effects of SJ contributions we present in Fig. 10 the predicted inclusive cross sections of $\pi^-\mathrm{Cu} \to \Lambda X$ and $\pi^-\mathrm{Cu} \to \Omega^- X$ reactions with (solid curves) and without (dashed curves) SJ contributions shown in Fig. 4c. We discuss precisely these reactions because the secondary baryons and the correspondent antibaryons $\bar{\Lambda}$ and $\overline{\Omega}^+$ have symmetrical quark

states in respect to the incident π^-. So the SJ contribution, which is equal to the difference between solid and dashed curves in Fig. 10, can be measured experimentally as the difference in $\Lambda - \bar{\Lambda}$, or $\Omega^- - \overline{\Omega}^+$ production at high energies.

In general, the SJ contribution shown in Fig. 4c increases the inclusive cross sections of Λ and Ω^- production. The spectra of antibaryons are not affected. However, numerically these effects are rather small, for example, mean multiplicity of secondary Λ in forward hemisphere should increase in about 15% that should be compensated by the correspondent decrease of secondary nucleon multiplicity in the target fragmentation region.

6 Comparison with the nuclear target data

In Fig. 11, we show the data [53] on the midrapidity inclusive densities, dn/dy at $|y_{c.m.}| < 0.5$ of secondary Λ, $\bar{\Lambda}$, Ξ^-, $\overline{\Xi}^+$ and the sum $\Omega^- + \overline{\Omega}^+$ produced in pBe and pPb collisions at 158 GeV/c. These data are in reasonable agreement with the QGSM calculations [54] and this agreement is better with the account for the SJ contributions for secondary baryons.

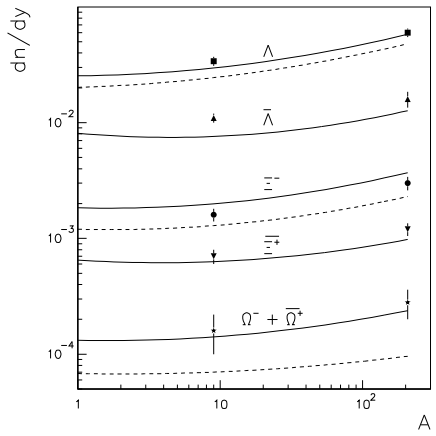


Figure 11: Yields of Λ (closed squares), $\bar{\Lambda}$ (triangles), Ξ^- (points), $\overline{\Xi}^+$ (turned over triangles) and the sum $\Omega^- + \overline{\Omega}^+$ (stars) per unit of rapidity at central rapidity as a function of the target atomic weight for pA collisions at 158 GeV/c. The QGSM predictions with SJ contribution are shown by solid curves and without SJ contribution by dashed curves

Similarly to the case of a nucleon target, the SJ effects are more important in the meson beam fragmentation. In Fig. 12 we present the NA49 Coll.

data [22] on the x_F distributions of net protons $(p - \bar{p})$ produced in πp and πPb interactions at $\sqrt{s} = 17.2\,\mathrm{GeV}$. The beam π is determined in [22] as $(\pi^+ + \pi^-)/2$. The data are described rather good [54] with the account for the SJ diffusion (solid curves in Fig. 12) and the variant without SJ contribution (dashed curves) underestimates the data in several times at $x_F > 0.1$.

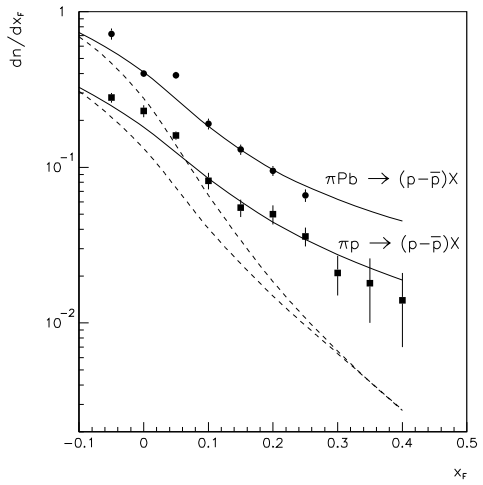


Figure 12: Feynman-x distributions of net protons produced in πp (squares) and πPb (points) interactions at $\sqrt{s} = 17.2\,\mathrm{GeV}$. Solid and dashed curves show the QGSM description with and without SJ contribution, respectively

The experimental data of WA89 Coll. [23] on Λ, Ξ^-, $\bar{\Lambda}$ and $\overline{\Xi}^+$ production from C and Cu targets by $345\,\mathrm{GeV/c}$ π^- beam are shown in Fig. 13. The yields of secondary hyperons are in reasonable agreement with QGSM predictions [54] accounting for the SJ contributions (solid curves in Figs. 13a and 13b). The calculations without SJ contributions (dashed curves) disagree with the data.

The yields of $\bar{\Lambda}$ and $\overline{\Xi}^+$ [23], which do not depend on SJ contribution, are shown in Fig. 13c. These data are described by QGSM on the reasonable level.

The data presented in [23] allow one to calculate the asymmetries of secondary $\Lambda/\bar{\Lambda}$ production defined by Eq. (17). They are presented in Fig. 14a for the cases of π^-Cu (points) and π^-C (squares) interactions. The curves show the QGSM calculations [54] for copper (dotted curve), carbon (dashed curve) and nucleon (solid curve) targets. We predict some A-dependence of the asymmetry for beam fragmentation region. The agreement with the data is reasonable in the central region, but we obtain some underestimation of

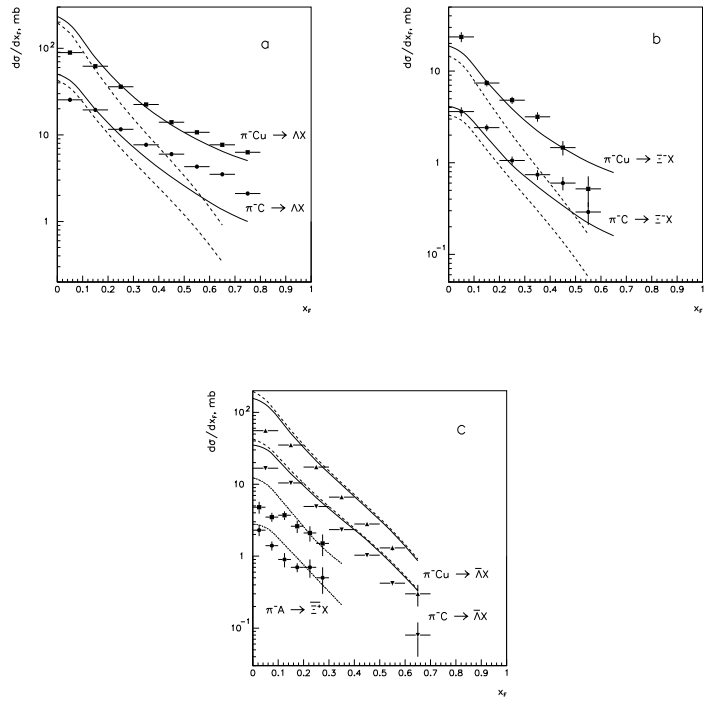


Figure 13: Feynman-x distributions of secondary Λ (a), Ξ^- (b), $\bar{\Lambda}$ and $\overline{\Xi^+}$ (c) produced in π^-C and π^-Cu interactions at 345 GeV/c. Solid and dashed curves show the QGSM prediction for secondary hyperon spectra with and without SJ contribution

asymmetry for $x_F > 0.3$.

In Fig. 14b we present the data of [55] for the same asymmetry Eq. (17) obtained for π^- interactions with multifoil target with different atomic weights, see [55]. Here the QGSM predictions [32, 54] even for $\pi^- p$ interactions (solid curve), *i.e.* neglecting the A-dependence, overestimate the data at $x_F > 0.1$. In the central region, $|x_F| \leq 0.1$, our calculations agree with the data of both [23] and [55] as well as of [20]. Here we predict the practical absence of A-dependence (or weak dependence) for $\Lambda/\bar{\Lambda}$ asymmetries, as it was assumed in [32]. In the π^- fragmentation region the data of [23] and [55] are in strong disagreement with each other.

The comparison of data shown in Figs. 13a and 13c allows us to obtain the direct results for SJ contribution to hyperon production cross section. Really, Λ has the valence quark content uds, so the fast incident π^- ($\bar{u}d$) should fragment into secondary Λ and $\bar{\Lambda}$ with equal probabilities, *i.e.* the $\pi^- \to$

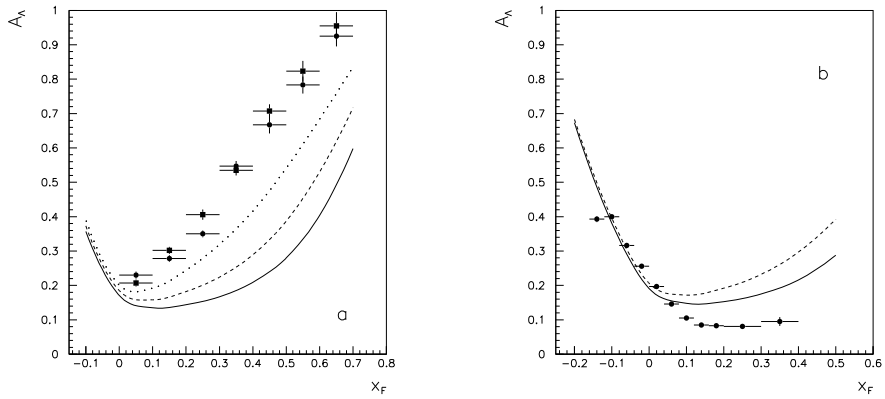


Figure 14: The asymmetries of secondary $\Lambda/\bar{\Lambda}$ production in π^-C (squares) and π^-Cu (points) interactions at 345 GeV/c (a). The same asymmetries for $\pi^- A$ collisions at 250 GeV/c (b). Solid, dashed and dotted curves show the QGSM predictions for nucleon, carbon and copper targets, respectively

$\Lambda, \bar{\Lambda}$ fragmentation is flavour symmetrical, contrary, say, to the $\pi^- \to p, \bar{p}$ fragmentation.

So the contributions of the processes of Figs. 4a and 4b are negligible at $x_F > 0.1$ and the difference in the spectra of secondary Λ and $\bar{\Lambda}$ determines the SJ contribution of the process shown in Fig. 4c. This difference is obtained to be rather large in [23] (in the case of nuclear targets) but very small in [56] (for $\pi^- p$ collisions). To show the disagreement between the data of [23] and [56] we present in the Table 1 the values of the parameter n for the parametrization

$$d\sigma/dx_F \;=\; C(1-x_F)^n, \tag{21}$$

which were obtained in [23] and [56] for secondary Λ and $\bar{\Lambda}$ production.

The values of n for the secondary Λ production obtained both in [23] and [56] on nucleon and on nuclear targets are in agreement, with a natural weak A-dependence. The value of n slightly increases with A that demonstrate well-known effect of nuclear absorption [5],[37]–[39]. The values of n for $\bar{\Lambda}$ production obtained in [56] and [23] are absolutely different. The data of [56] show the absence, or very small contribution of SJ diffusion in the case of Λ and $\bar{\Lambda}$ production, in contradiction with [23] and with several another results, see, for example, [20, 34].

It is possible to extract the SJ contribution from the experimental data of [23]. At positive x_F the condition $x_F > 0.1$ for π^- beam at 345 GeV/c means

Table 1: The values of the parameter n in Eq. (21) obtained in [56] and [23] for Λ and $\bar{\Lambda}$ production in high energy $\pi^- p$ and $\pi^- A$ collisions

Reaction	n
$\pi^- p \to \Lambda$ [56]	2.0 ± 0.1
π^-C $\to \Lambda$ [23]	2.12 ± 0.02
π^-Cu $\to \Lambda$ [23]	2.71 ± 0.02
$\pi^- p \to \bar{\Lambda}$ [56]	2.0 ± 0.1
π^-C $\to \bar{\Lambda}$ [23]	5.23 ± 0.04
π^-Cu $\to \bar{\Lambda}$ [23]	5.53 ± 0.04

$y - y_{\rm target} > 4$ for secondary Λ, *i.e.* these Λ are rather far from the target nucleons in rapidity space. So the difference between the yields of secondary Λ and $\bar{\Lambda}$ comes from the SJ contribution shown in Fig. 4c. The SJ contributions to the spectrum of secondary Λ in π^-Cu and π^-C collisions, obtained by such a way are presented in Fig. 15.

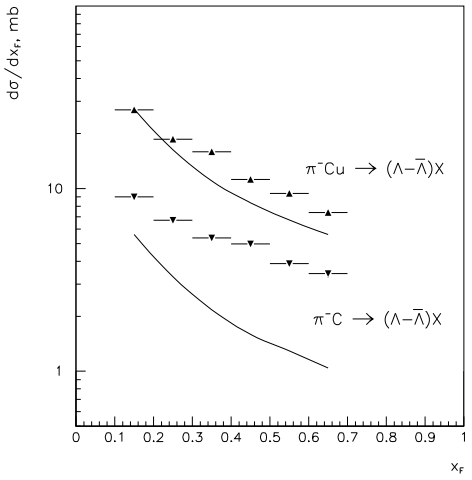


Figure 15: The extracted SJ contributions to the spectra of Λ in $\pi^- A$ collisions at 345 GeV/c and their description by QGSM

The x_F-distributions of the Λ produced from copper target are in reasonable agreement with QGSM calculations, however in the case of carbon target we obtain the disagreement coming mainly from not good description in Fig. 13a and some overestimation of $\bar{\Lambda}$ production in Fig. 13c. It is necessary to note that the data [56] leads to very small SJ contribution.

In Fig. 16 the dependence of $\bar{p}/p$ ratios at $|y_{c.m.}| = 0$ is shown as a function of "centrality" (ν) in dAu collisions at $\sqrt{s} = 200\,\mathrm{GeV}$ [57]. The experimental data are shown here by open squires and the QGSM predictions with SJ contribution by the solid curve which is very close to the constant. The reason for such behaviour is that the energy is high enough, so both the spectrum of $\bar{p}$ and the contribution of SJ diffusion to the proton spectrum from the target nucleons are approximately proportional to ν. As a result their ratio is practically ν-independent. The calculation without SJ contribution (dashed curve in Fig. 16) is also practically constant, but it again leads to high values of $\bar{p}/p$ ratios similarly to the case shown in Fig. 6. The close points in Fig. 16 present the predictions of the DPMJET-III model [58] and they are in agreement with the data, as well as with QGSM calculations. Dash–dotted curve in Fig. 16 shows the QGSM predictions for $\bar{\Lambda}/\Lambda$ ratios.

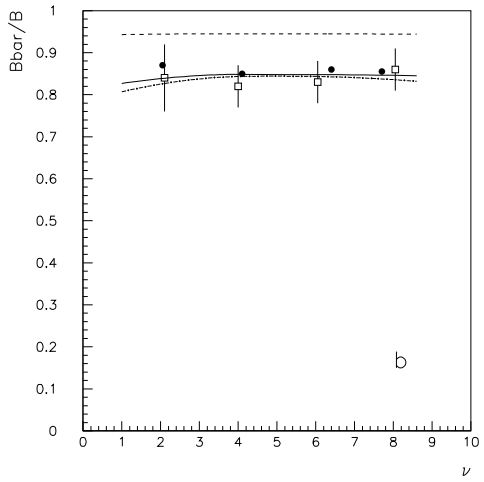


Figure 16: The experimental $\bar{p}/p$ ratio as a function of "centrality" for dAu collisions at $\sqrt{s} = 200\,\mathrm{GeV}$ (open squares) together with the QGSM calculations with SJ (solid curve) and without SJ (dashed curve) and with the DPMJET-III model (closed points) predictions. The QGSM predictions for $\bar{\Lambda}/\Lambda$ ratio are shown by dash–dotted curve

The predictions of several another models [59]–[61] are in some disagreement with the data of [57] (see Fig. 4 in [57]). The extrapolation of the predictions of these models to $\nu = 1$ give the values of $\bar{p}/p$ in pp interactions larger than 0.9 that contradicts the data presented both in Figs. 6 and 16.

7 Conclusion

We discuss the role of string junction diffusion for the baryon charge transfer over large rapidity distances for the cases of collisions with nucleon and nuclear targets. The accounting for the SJ contribution shown in Fig. 4c with parameters (15) allows one to describe, on a reasonable level, the main piece of the existing experimental data. The calculations of the baryon/antibaryon yields and asymmetries without SJ contribution disagree with the most experimental data, where this contribution should be important. The discussed string junction effects has A-dependences which in general agree with the QGSM predictions (see, for example, Figs. 11 and 13).

It is necessary to note that the existing experimental data are not enough for determination of the SJ parameters with the needed accuracy. Certain data disagree with the other ones, for example, the experimental behaviour of $\bar{\Lambda}$ spectra at $x_F > 0$ obtained by [56] and [23], see Table 1, and the experimental $\Lambda/\bar{\Lambda}$ asymmetries in [23] and [55] which are presented in Figs. 14a and 14b. There exists a disagreement in yields of secondary protons with $x_F = 0$ produced in pp collisions which were measured in [24] and [52].

We are grateful to G. H. Arakelyan, F. Bopp, A. Capella, A. B. Kaidalov, L. N. Lipatov, C. Merino, O. I. Piskounova, M. G. Ryskin and A. A. Rostovtsev for useful discussions. This paper was supported by DFG grant GZ: 436 RUS 113/771/1-2 and, in part, by grants RSGSS-1124.2003.2 and PDD (CP) PST.CLG980287.

References

[1] A.B. Kaidalov, K.A. Ter-Martirosyan, Yad. Fiz. **39**, 1545 (1984); **40**, 211 (1984).

[2] A.B. Kaidalov, O.I. Piskunova, Yad. Fiz. **41**, 1278 (1985).

[3] A. Capella, U. Sukhatme, C.I. Tan, J. Tran Thanh Van, Phys. Rep. **236**, 225 (1994).

[4] A. Capella, J. Tran Thanh Van, Z. Phys. C **10**, 249 (1981).

[5] A.B. Kaidalov, K.A. Ter-Martirosyan and Yu.M. Shabelski, Yad. Fiz. **43**, 1282 (1986).

[6] Yu.M. Shabelski, Yad. Fiz. **44**, 186 (1986).

[7] Yu.M. Shabelski, Nucl. Phys. Proc. Suppl. B **52**, 116 (1997).

[8] V.A. Abramovsky, V.N. Gribov and O.V. Kancheli, Yad. Fiz. **18**, 595 (1973).

[9] A.B. Kaidalov, Sov. J. Nucl. Phys. **45**, 902 (1987); Yad. Fiz. **43**, 1282 (1986).

[10] X. Artru, Nucl. Phys. B **85**, 442 (1975).

[11] M. Imachi, S. Otsuki and F. Toyoda, Prog. Theor. Phys. **52**, 346 (1974); **54**, 280 (1976); **55**, 551 (1976).

[12] G.C. Rossi, G. Veneziano, Nucl. Phys. B **123**, 507 (1977).

[13] L. Montanet, G.C. Rossi and G. Veneziano, Phys. Rep. **63**, 149 (1980).

[14] D. Kharzeev, Phys. Lett. B **378**, 238 (1996).

[15] M. Imachi, S. Otsuki and F. Toyoda, Progr. Theor. Phys. **57**, 517 (1977).

[16] M. Imachi, S. Otsuki and F. Toyoda, Prog. Theor. Phys. **52**, 715 (1974).

[17] M. Imachi, S. Otsuki and F. Toyoda, Prog. Theor. Phys. **55**, 1211 (1976).

[18] H. Kanada *et al.*, Progr. Theor. Phys. **59**, 2162 (1978).

[19] H. Noda, Progr. Theor. Phys. **68**, 1406 (1982).

[20] E.M. Aitala *et al.*, E769 Coll., hep-ex/0009016; Phys. Lett. B **469**, 9 (2000).

[21] A.E. Brenner *et al.*, Phys. Rev. D **26**, 1497 (1982).

[22] H.G. Fischer, NA49 Coll., Nucl. Phys. A **715**, 118 (2003); hep-ex/0209043.

[23] M.I. Adamovich *et al.*, WA89 Coll., Z. Phys. C **76**, 35 (1997); Eur. Phys. J. C **26**, 357 (2003).

[24] M. Banner *et al.*, Phys. Lett. B **41**, 547 (1972);
B. Alper *et al.*, Nucl. Phys. B **100**, 237 (1975).

[25] I.G. Bearden *et al.*, BRAHMS Coll., Phys. Lett. B **607**, 42 (2005); nucl-ex/0409002.

[26] B.H. Samset *et al.*, BRAHMS Coll., Submitted to the Quark Matter 2004 Int. Conf., Oakland, Jan. 2004.

[27] C. Adloff *et al.*, H1 Coll., Submitted to the 29th Int. Conf. on High Energy Physics ICHEP98, Vancouver, July 1998.

[28] B.Z. Kopeliovich and B. Povh, Z. Phys. C **75** (1997) 693.

[29] B.Z. Kopeliovich and B. Povh, Phys. Lett. B **446** (1999) 321.

[30] G.T. Garvey, B.Z. Kopeliovich and B. Povh, Comments Mod. Phys. A **2**, 47 (2001); hep-ph/0006325.

[31] F. Bopp, hep-ph/0002190; hep-ph/0007229.

[32] G.H. Arakelyan, A. Capella, A.B. Kaidalov and Yu.M. Shabelski, Eur. Phys. J. C **26**, 81 (2002); hep-ph/0103337.

[33] F. Bopp and Yu.M. Shabelski, Yad. Fiz. **68**, 2155 (2005); hep-ph/0406158.

[34] G.H. Arakelyan, C. Merino and Yu.M. Shabelski, Yad. Fiz. **69**, 911 (2006); hep-ph/0505100.

[35] G.H. Arakelyan, C. Merino and Yu.M. Shabelski, hep-ph/0604103.

[36] O.I. Piskounova, Proc. of the HERA-LHC Workshop, DESY, March 2005.

[37] Yu.M. Shabelski, Nucl. Phys. B **132**, 491 (1978).

[38] A. Capella and A. Krzywicki, Phys. Rev. D **18**, 3357 (1978).

[39] V.V. Anisovich, Yu.M. Shabelski and V.M. Shekhter, Yad. Fiz. **28**, 1063 (1978); Nucl. Phys. B **133**, 477 (1978).

[40] V.G. Bornyanov *et al.*, Uspekhi Fiz. Nauk **174**, 19 (2004).

[41] G. Veneziano, Nucl. Phys. B **117**, 519 (1976).

[42] S. Fleck *et al.*, Phys. Lett. B **220**, 616 (1989).

[43] D. Diakonov, V. Petrov and M. Polyakov, Z. Phys. A **359**, 305 (1997).

[44] I.M. Narodetskii, Yad. Fiz. **68**, 780 (2005).

[45] E.M. Levin and L.L. Frankfurt, Pisma v ZhETF **2**, 105 (1965); H.J. Lipkin and F. Scheck, Phys. Rev. Lett. **16**, 71 (1966).

[46] V.V. Anisovich, M.N. Kobrinsky, J. Nyiri and Yu.M. Shabelski, Soviet Physics – Uspekhi **144**, 553 (1984); *Quark Model and High Energy Collisions*, World Scientific, Singapore, 1985.

[47] B. Muller and J.L. Nagle, nucl-th/0602029.

[48] V.V. Anisovich and V.M. Shekhter, Nucl. Phys. B **55**, 455 (1973).

[49] A. Capella and C.-A. Salgado, Phys. Rev. C **60**, 054906 (1999).

[50] B.Z. Kopeliovich and B.G. Zakharov, Phys. Lett. B **211**, 221 (1988); E. Gotsman and S. Nusinov, Phys. Rev. D **22**, 624 (1980).

[51] A. Capella and B.Z. Kopeliovich, Phys. Lett. B **381** 325 (1996).

[52] M. Aguilar-Benitez *et al.*, LEBC-EHS Coll. Z. Phys. **50** 405 (1991).

[53] F. Antinori *et al.*, WA97 Coll., Nucl. Phys. B **681**, 141 (2001).

[54] F. Bopp and Yu.M. Shabelski, Eur. Phys. J. A **28**, 237 (2006); hep-ph/0603193.

[55] G.A. Alves *et al.*, E769 Coll., Phys. Lett B **559**, 179 (2003); hep-ex/0303027.

[56] S. Mikocki *et al.*, Phys. Rev. D **34**, 42 (1986).

[57] B.B. Back *et al.*, PHOBOS Coll., Phys. Rev. C **70**, 011901 (2004); nucl-ex/0309013.

[58] F.W. Bopp, J. Ranft, R. Engel and S. Roesler, hep-ph/0505035.

[59] M. Gyulassy and X.N. Wang, Comput. Phys. Commun. **83**, 307 (1994).

[60] H. Sorge, Phys. Rev. C **52**, 3291 (1995).

[61] Z. W. Lin *et al.*, Phys. Rev. C **64**, 011902 (2001); B. Zhang *et al.*, Phys. Rev. C **61**, 067901 (2000).